

## Heteroepitaxial growth of MgO(111) thin films on Al<sub>2</sub>O<sub>3</sub>(0001): Evidence of a wurtzite to rocksalt transformation

Carlos Martínez-Boubeta,<sup>1,\*</sup> Antía S. Botana,<sup>2,3</sup> Victor Pardo,<sup>2,3</sup> Daniel Baldomir,<sup>2,3</sup> Aldrin Antony,<sup>4</sup> Joan Bertomeu,<sup>4</sup> Josep M. Rebled,<sup>1</sup> Lluís López-Conesa,<sup>1</sup> Sonia Estradé,<sup>1</sup> and Francesca Peiró<sup>1</sup>

<sup>1</sup>Departament d'Electrònica and IN2UB, Universitat de Barcelona, Martí i Franquès 1, 08028 Barcelona, Spain

<sup>2</sup>Departamento de Física Aplicada, Universidade de Santiago de Compostela, 15782 Santiago de Compostela, Spain

<sup>3</sup>Instituto de Investigacións Tecnolóxicas, Universidade de Santiago de Compostela, 15782 Santiago de Compostela, Spain

<sup>4</sup>Grup d'Energia Solar, Departament de Física Aplicada i Òptica, Universitat de Barcelona, 08028 Barcelona, Spain

(Received 30 April 2012; revised manuscript received 2 June 2012; published 19 July 2012)

We report on a growth study of MgO films deposited on Al<sub>2</sub>O<sub>3</sub>(0001) substrates by magnetron sputtering. The films exhibited a preferred rocksalt MgO(111) orientation. Surprisingly, depending on the O<sub>2</sub> gas flow ratio, a structure of graphiticlike wurtzite MgO(0001) has been revealed. The observed Mg-O perpendicular bond length reduction is accompanied by an atomically flat surface morphology for the development of MgO(111) films; the transition to the bulk rocksalt structure occurs in the 3–6 nm coverage range. Previously, relaxation of the electrostatic instability of MgO(111) films accompanied by an in-plane lattice increase has been suggested theoretically [*Phys. Rev. Lett.* **98**, 205701 (2007)]. Here, relying on *ab initio* calculations, we infer that Mg vacancies facilitate the lattice match with the substrate. This mechanism suggests methods to engineer oxide heterostructures.

DOI: 10.1103/PhysRevB.86.041407

PACS number(s): 61.72.-y, 71.15.Ap, 77.55.Px

Nanoscale alkaline earth metal oxides, in particular, MgO, are very promising materials for applications as adsorbents for decontaminating wastewater due to their favorable electrostatic attraction mechanism, and the simplicity of their production from abundant natural minerals.<sup>1</sup> Furthermore, the MgO(111) facet, which not only presents the largest number of dangling bonds per atom, but also alternating layers of O<sup>2-</sup> and Mg<sup>2+</sup>, and thus, a strong electrostatic field, is obviously anticipated to be more reactive, compared to nonpolar surfaces. In this regard, recent studies on MgO(111) have suggested that the polar oxide surface may be of interest for the catalytic splitting of water and for hydrogen storage.<sup>2</sup> On the other hand, there is an increasing interest in the growth of high quality MgO films because of their unique physical properties which allow the fabrication of buffered epitaxial layers of ferroelectric materials and superconductors, as well as wide-band-gap semiconductors for many optoelectronic applications.<sup>3</sup> MgO(111) layers are also interesting for the exploitation of spintronic devices.<sup>4</sup> Therefore, it remains a great challenge to develop general methods for the controllable growth of unusual (111) exposed MgO crystal surfaces. Such a surface has attracted a great deal of attention from both experimental and theoretical studies.<sup>5–19</sup>

In spite of the large number of studies made, many features of this process are not yet understood. Therefore, the investigations described herein are aimed at better understanding the microstructural details of MgO(111) films. To this end, MgO thin films were grown on Al<sub>2</sub>O<sub>3</sub>(0001) (“c-plane sapphire”) substrates by sputtering deposition. While bulk MgO has a six-coordinated rocksalt (B1) crystal structure with a lattice constant  $a = 0.421$  nm, the Al<sub>2</sub>O<sub>3</sub> is rhombohedral ( $a = 0.476$  nm,  $c = 1.299$  nm). As a result, the epitaxy of MgO films on sapphire is not straightforward. There are several experiments showing that (111)-oriented MgO can be accommodated onto sapphire(0001), since it offers the lowest substrate-to-film in-plane lattice mismatch (about 8%). One possible mechanism

is that growth proceeds by matching domains with a film-to-substrate lattice ratio of 4:5.<sup>20</sup> However, these (111) polar films are intrinsically unstable. Several mechanisms, including vacancy formation, hydroxylation, surface reconstruction, and metallization at the interface (despite the insulating character of the bulk material), have been proposed to account for the stabilization of such a polar catastrophe. Another possibility stems in the formation of the four-coordinate B4 (wurtzite) phase at the interface. Density functional theory (DFT) calculations predict that MgO with a B4 phase at the interface is far more stable.<sup>21</sup> In addition, tensile strain would induce a compression of the film along the wurtzite  $c$  axis, thus resulting in a nonpolar graphiticlike  $B_{\text{hex}}$ (0001) phase at low thickness.<sup>7,8,22</sup> According to these calculations, the  $c/a$  ratio is close to 1.2, which implies that the Mg and O atoms lie almost in the same plane. Despite theoretical predictions and their great importance for thin film stabilization, as well as potential applications, compelling evidence is still needed.

Furthermore, the cited DFT calculations predict a nonzero density of states in the gap,<sup>7,12</sup> suggestive of ferromagnetic instability. In this scope, our interest in MgO stems partly from the increasing evidence that magnetic order can be triggered by certain defects.<sup>23</sup> Particularly, the magnetic moments of the system arise from the spin polarization of the  $2p$  states of oxygen atoms neighboring Mg vacancies, the spatially spread  $3s$  orbitals of adjacent cations enabling the exchange interaction between those local moments, eventually enhanced by lattice distortions.<sup>24,25</sup>

Motivated by these findings, we explore here the possibility of stabilizing MgO(111) layers on sapphire by rf-magnetron sputtering. MgO (<100 nm) films were deposited from a >99.99% purity MgO single crystal target (Semiconductor Wafer, Inc., Taiwan) at 50 W power for 90 min. Prior to growth, the substrate (MTI Corporation, Richmond, CA) was thermally outgassed at 500 °C in the vacuum chamber (base pressure  $4 \times 10^{-6}$  mbar) for 1 h. Oxygen was then introduced and

the temperature lowered. The growth temperature was  $450^\circ\text{C}$ , while the growth pressure was  $5 \times 10^{-4}$  mbar. Previously, we have reported on the tuning of the magnetic properties by using growth conditions to control the density of vacancies within the MgO.<sup>26</sup> In the present Rapid Communication, we have deposited films by increasing the oxygen gas flow from 50 sccm (sample 1) to 300 sccm (sample 3) while diminishing the Ar partial pressure. In order to consider the possible stabilizing effect of water adsorption on the polar MgO{111} face,<sup>6,18</sup> we have also deposited MgO using 200 sccm  $\text{O}_2$  (sample 2) while the remaining partial pressure was made up by  $\text{H}_2\text{O}$  vapor. Water enables the generation of reactive oxygen species but also OH and  $\text{H}_2\text{O}_2$ .<sup>27</sup> Finally, the growth process included a cooling down step to room temperature (about an hour) under an oxygen flow of 300 sccm, in an attempt to reduce the concentration of oxygen defects in the films. After growth, the film orientation, morphology, and structure were investigated by x-ray diffraction (XRD) and reflectometry (XRR) measurements using  $\text{Cu } K\alpha$  radiation, whereas cross-sectional imaging was additionally used by means of a Jeol 2010F field-emission gun microscope. For three-dimensional atomic modeling we used the RHODIUS software. *Ab initio* calculations were performed using the WIEN2K code,<sup>28</sup> based on DFT utilizing the augmented plane wave plus local orbitals method.<sup>29</sup> The exchange-correlation potential utilized was the Wu-Cohen version of the generalized gradient approximation<sup>30</sup> that has been shown to yield accurate structural parameters for *sp* semiconductors.<sup>31</sup> All calculations were fully converged with respect to the *k* mesh (up to  $12 \times 12 \times 12$  for the bulk cases) and  $R_{\text{mt}}K_{\text{max}}$  (up to a value of 7.0, with smaller muffin-tin radii of 1.69 for O).

Figure 1 shows XRD spectra for the MgO thin films on  $\text{Al}_2\text{O}_3(0001)$ . It can be seen that only (111) and (222) reflections of MgO thin films were obtained. The full width at half maximum of the MgO(111) peak is about  $0.27^\circ$ , indicating high crystal quality. On the other hand, despite the fact that no appreciable differences were perceptible in  $\theta$ - $2\theta$  scans, the impact of hydroxylation on the film quality is noticeable in the increased mosaic spread (from  $3^\circ$  up to  $5.3^\circ$ ) of the  $\omega$ -rocking curves [inset of Fig. 1(a), which inversely relates to the quality of the out-of-plane texture]. However, conclusive proof of the heteroepitaxial character and crystal quality of the MgO(111) is given in Fig. 1(b), where the in-plane  $\phi$  scans further indicate that films of better crystallinity were found to be grown in an Ar assisted plasma. It is also worth mentioning that these MgO films show a sixfold symmetry. In principle, trigonal substrates such as *c*-plane  $\text{Al}_2\text{O}_3(0001)$  offer a  $3m$  point symmetry, though elemental steps on this surface give rise to a  $60^\circ$  rotation of the adatom site symmetry on the neighboring terraces. Therefore, the growth of threefold symmetric materials, such as cubic (111)-oriented crystals, onto  $3m$  substrates is expected to yield two orientation variants,<sup>32</sup> as shown here.

Important differences have been obtained in the XRR measurements. In the bottom panel of Fig. 1, we show XRR curves and their corresponding best fits for the series of samples. X-ray reflectivity data were fitted using commercial software, thus giving information about the layers' thicknesses and interface roughnesses. In all cases the interfaces were modeled with a Gaussian profile. We note a root-mean-square roughness of nearly 1.5 nm, which is characteristic of polar

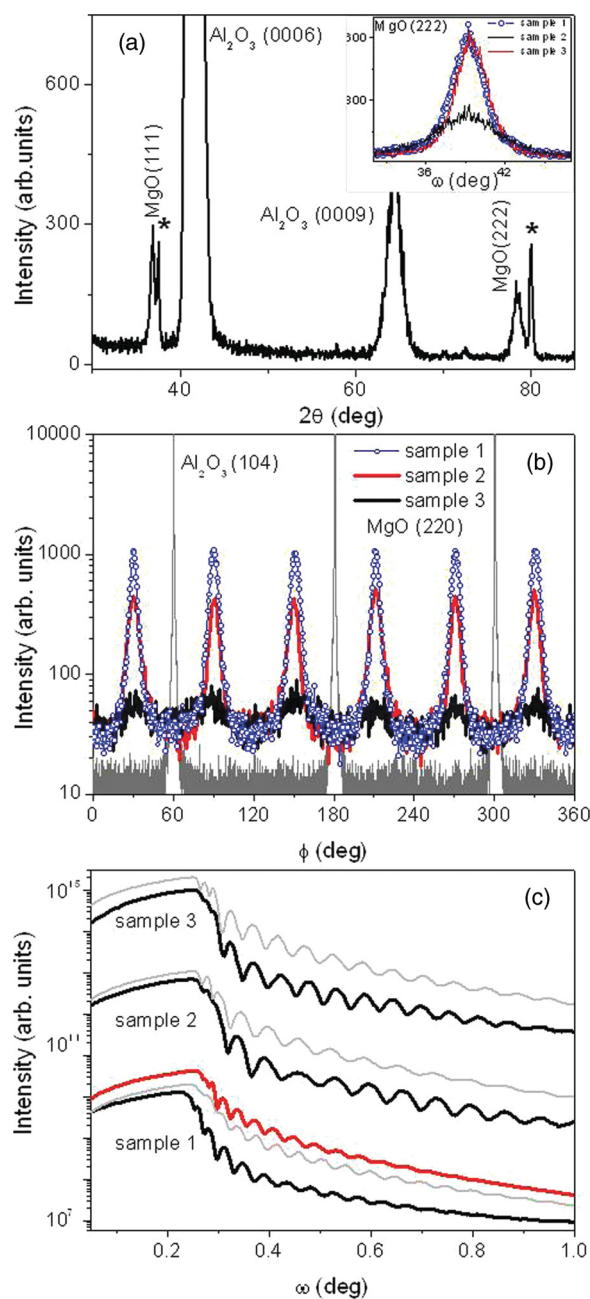


FIG. 1. (Color online) (a) High-angle XRD pattern. Asterisk (\*) denotes  $K\beta$  peaks from the sapphire substrate. The inset shows  $\omega$  rocking curves of MgO(222) diffraction peaks. Sample 1 corresponds to films deposited in an Ar/ $\text{O}_2$  (50 sccm) plasma, sample 2 to  $\text{H}_2\text{O}/\text{O}_2$  (200 sccm), and sample 3 to Ar/ $\text{O}_2$  (300 sccm). (b) In-plane  $\phi$  scans of asymmetric MgO(220) and sapphire (1-104) peaks. (c) Specular XRD profiles (black curves) of samples in the low angle region, together with best fits (gray curves) if an abrupt transition occurs from the MgO thin film to sapphire substrate. The curves are offset for clarity. The calculated spectrum including an interface layer is also shown for sample 1 (red thick curve). Thicknesses were estimated to be 82 nm (sample 1), 58 nm (sample 2), and 67 nm (sample 3).

*c*-plane sapphire substrates, though the deposited MgO films showed a top surface flatness of the order of elementary steps. It appears that the surface roughness (about 0.27 nm for samples 1 and 2, compared to 0.45 nm for sample 3)

is increased by increasing the oxygen partial pressure, while the films become flatter when water is added to the reaction gas. Noteworthy, in the XRR simulation the MgO density is found to be slighter than that from bulk (about 3.20 vs 3.58 g/cm<sup>3</sup>), which is taken as an indication of the existence of cation vacancies in our samples. The growth rate decreased from 0.91 to 0.64 nm/min due to a decrease in the sputtering yield when replacing part of the Ar with the lighter O<sub>2</sub> and H<sub>2</sub>. A similar decrease of the growth rate is observed when decreasing the sputtering power density, which in turn was shown to minimize the number of cation vacancies in MgO films.<sup>26</sup> We might thus speculate that the diminished critical angle for total reflection appearing for sample 1, and hence its depleted electronic density, is a consequence of the higher amount of cation vacancies in this sample as a result of the highest deposition rate, as already demonstrated by means of luminescence spectroscopy.<sup>33</sup> Support is also given from the induced *p*-type semiconductivity in related films.<sup>34</sup>

Concomitantly, it is quite striking that best fits for XRR data shown in Fig. 1(c) reasonably reproduce the experimental curves, except for sample 1. Let us now focus our attention on this sample. Here, we added an inner layer in the XRR simulation in order to account for the hypothetical formation of MgAl<sub>2</sub>O<sub>4</sub> at the interface. The spinel-forming solid state reaction MgO + Al<sub>2</sub>O<sub>3</sub> → MgAl<sub>2</sub>O<sub>4</sub> can easily proceed upon heating, and it is one of the mechanisms that might help to relax the electrostatic instability of MgO(111) at the sapphire interface. However, MgAl<sub>2</sub>O<sub>4</sub> can be safely discarded since the 3 nm interlayer explaining the reflectometry in sample 1 results in a density below that of MgO bulk. In fact, the sharp MgO/Al<sub>2</sub>O<sub>3</sub> interface could be anticipated from the temperatures used in our experiments, well below the limit of 1000 °C for spinel formation.<sup>35</sup> Morphological changes in the MgO(111) surface therefore remain as the most likely mechanism to suppress uncompensated polarity. Cross-sectional imaging provides evidence for several structural modifications. Figure 2 shows a general transmission electron microscopy view and selected area electron diffractions (SAEDs) of the MgO film (sample 1) grown onto the sapphire substrate. Analysis reveals the MgO(111)/Al<sub>2</sub>O<sub>3</sub>(0001) films to have an in-plane MgO[1-10]//Al<sub>2</sub>O<sub>3</sub>[1-100] relationship, in con-

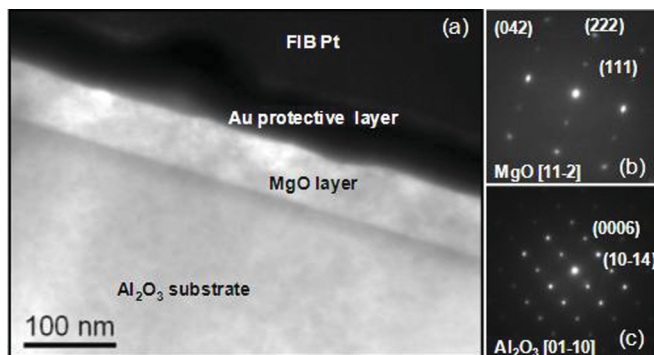


FIG. 2. (Color online) (a) Electron micrograph of the MgO film grown on the *c*-plane sapphire. A focused ion beam instrument was used to create the cross section of the sample. (b) Selected area electron diffraction pattern along the [11-2] axis of the MgO, and (c) along the [01-10] in the sapphire region.

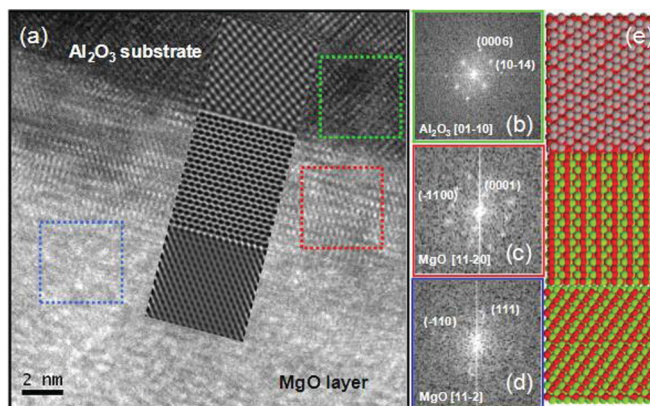


FIG. 3. (Color online) (a) HRTEM detail of the MgO/Al<sub>2</sub>O<sub>3</sub> interface with a transition stage from (111) to MgO(0001). The framed area is a simulated image of MgO rocksalt on *c*-plane sapphire with a distorted wurtzite (graphitelike) buffer layer. (c), (d) Power spectra (FFT) obtained on the squared areas in (a). (e) Atomic model used in the HRTEM simulation. O (red), Mg (green), and Al (purple) are represented by different ball sizes in ascending order. It is interesting to note that the MgO growth proceeds at the O-terminated sapphire surface, as anticipated in Ref. 11.

cordance with XRD measurements. In spite of high sample susceptibility to the electron beam, it was possible to obtain a high resolution transmission electron microscopy (HRTEM) image of the MgO/Al<sub>2</sub>O<sub>3</sub> interface. It is apparent from Fig. 3 that about 4.5 nm neighboring the interface seems to correspond to wurtzite MgO growing along the (0001) direction.<sup>11</sup> It then changes to rocksalt (111)-oriented MgO, in good agreement with SAED data. The interplane distance of (0001) and (-1100) planes are measured and labeled within this buffer layer as 0.46 and 0.28 nm, respectively [Fig. 3(c)]. Correspondingly, the calculated out-of-plane and in-plane lattice constants are about 0.46 and 0.396 nm. Interestingly enough, what it is found in this work is that the *c/a* = 1.16 parameters of MgO are thus very different from those in ideal wurtzite (*c/a* = 1.63),<sup>21</sup> which reveals the existence of a graphiticlike structure only a few nm away from the interface. For a clarification of the whole diffraction, Fig. 3(e) shows a geometrical construction for the MgO(111)/MgO(0001)/Al<sub>2</sub>O<sub>3</sub>(0001) stack. The multislice method was used to calculate the propagation of the electron wave through the projected atomic potential of the model. A computer simulation of the HRTEM image using the TEMsim software is also illustrated, and firmly corroborates the MgO graphiticlike interlayer.

Intuitively, since the electrostatic energy per area is lowered as the interlayer distance decreases, the out-of-plane lattice constant would tend to shrink in polar films. The energy landscape for this transformation has been proposed to stem from the epitaxial strain field at the interface.<sup>11,22</sup> Certainly, this structural modification may also result from changes in the concentration of cation vacancies within the oxide film.<sup>36</sup> Noteworthy, polar interfaces are known to have an extremely high concentration of structural vacancies;<sup>9,37</sup> in practice their value is a very sensitive function of the growth conditions. In this regard, calculations up to now have been performed on thin stoichiometric MgO(111), either unsupported<sup>8</sup> or

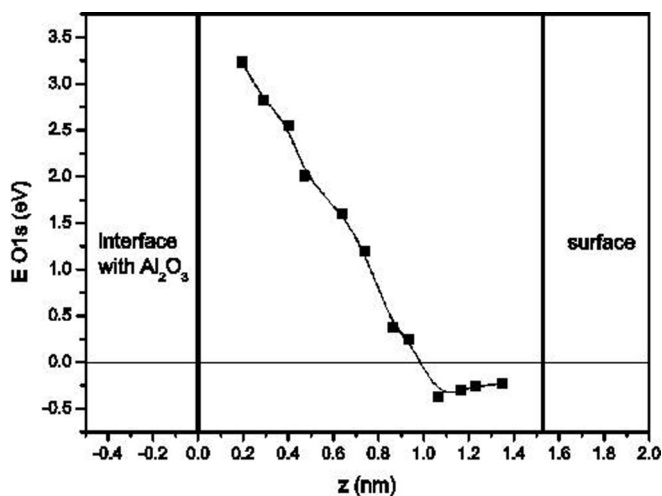


FIG. 4. Difference in energy of the O 1s core level inside the MgO slab compared with the bulk value (taken as  $\Delta E = 0$ ). Observe the convergence to an inner bulklike value at  $z > 1$  nm. Surface values (affected by the different Mg coordinations) are not shown for clarity.

deposited onto a weakly interacting metal substrate.<sup>9,12</sup> We first performed *ab initio* calculations on bulk stoichiometric hexagonal MgO, obtaining a  $c/a$  ratio of 1.20, very close to previous theoretical results,<sup>21</sup> though stoichiometric MgO samples on  $\text{Al}_2\text{O}_3$  would be strained (the area per cation is  $10.7 \text{ \AA}^2/\text{Mg}$  in hexagonal MgO and  $9.9 \text{ \AA}^2/\text{Al}$  in  $\text{Al}_2\text{O}_3$ ). We speculated that vacancies may allow for better lattice matching. Therefore, Mg and O vacancies were also included in the calculation. Results showed that a better lattice match between the  $\text{Al}_2\text{O}_3$  substrate and MgO occurs for Mg-deficient MgO. For the case of unsupported  $\text{Mg}_{0.75}\text{O}$  in the hexagonal structure, and considering only in-plane vacancies, there is a reduction in the lattice parameter from 0.351 to 0.345 nm, thus facilitating epitaxial growth. Corroborating this result, Kan *et al.* have calculated the cation vacancy concentration increases upon volume contraction.<sup>25</sup> Conversely, Matsuzaki *et al.*<sup>38</sup> have recently observed lattice expansion in oxygen-deficient MgO(111) films.

Following this, a computation of MgO/ $\text{Al}_2\text{O}_3$  in a layer-by-layer condition was performed using building blocks of six layer films separated by a region of vacuum thick enough to guarantee a lack of interaction between blocks. Previous calculations have shown that MgO in an ideal wurtzite structure ( $c/a = 1.6$ ) is unstable,<sup>39</sup> being metastable as a layered hexagonal phase in which Mg is approximately threefold coordinated, and with a  $c/a$  ratio shortened to 1.20. Such a structure would be almost nonpolar, and thus one would expect (and our calculations confirm) that growing MgO on

top of polar  $\text{Al}_2\text{O}_3$  leads to a distorted analog of this layered hexagonal structure. This hexagonal structure will survive for a few nm until the interface effects are no longer felt inside the MgO. In the structural relaxation of the multilayers we have calculated, it can be observed that MgO indeed gets further distorted in order to accommodate the appropriate cation-anion bonds across the interface with  $\text{Al}_2\text{O}_3$ . To quantitatively assert the morphology of the overlayer under the driven force of the substrate, Fig. 4 illustrates the shift of the O 1s core level inside the MgO block. This quantity reflects the change in the local environment of the anions towards a bulklike structure, at about 1 nm away from the interface. After a few nm (once all bulklike properties are recovered), the system will be able to relax to its energetically preferred rocksalt structure, as we have also observed experimentally. This situation is reminiscent of other thin film oxides, e.g.,  $\text{VO}_2$  needs about 5 nm to recover the bulklike properties,<sup>40</sup> whereas in calculations the O 1s core-level energy stabilizes about 1 nm away from the interface.<sup>41</sup>

In conclusion, growths of MgO epilayers on  $\text{Al}_2\text{O}_3(0001)$  surfaces were studied, where the structural properties of the crystals and the interfaces were compared. The MgO films grow in a rocksalt phase with their (111) axis aligned parallel to the substrate normal. We surmise that surface roughening is likely the main mechanism to suppress the emerging electrostatic dipoles (as shown for sample 3). Although hydroxilation indeed becomes relevant for suppressing the large surface dipole of the (111) surface, additional water largely reduced the roughness of MgO(111) films (sample 2), but at the expense of deteriorating the crystallinity. On the other hand, a HRTEM analysis of MgO films deposited at increased growth rates (sample 1) shows a graphiticlike structure at the interface, compressed along the  $c$  axis. Although it has been previously indicated that the metastable  $B_{\text{hex}}$  might have a lifetime that is too short to be resolved in the experiments,<sup>42</sup> our results show that in out-of-equilibrium processes with a high growth rate it is possible to freeze the wurtzite to rocksalt transformation. By means of density functional theory, the simulated O 1s core-level shifts in supported MgO enable a meaningful comparison with the measured interlayer thickness. This approach, combining microscopic crystallographic measurements together with deep insight into the electronic structure through *ab initio* calculations, opens wide prospects for a more complete understanding of polar thin films.

We appreciate valuable discussions with A. Cebollada. C.M.B. and V.P. gratefully acknowledge the financial support of the *Ramón y Cajal* program. A.S.B. thanks the Spanish FPU program.

\*Corresponding author: cmartinezboubeta@ub.edu

<sup>1</sup>J. Hu, Z. Song, L. Chen, H. Yang, J. Li, and R. Richards, *J. Chem. Eng. Data* **55**, 3742 (2010).

<sup>2</sup>K. Zhu, J. Hu, C. Kübel, and R. Richards, *Angew. Chem.* **118**, 7435 (2006).

<sup>3</sup>Y. Chen, H.-J. Ko, S.-K. Hong, and T. Yao, *Appl. Phys. Lett.* **76**, 559 (2000).

<sup>4</sup>R. Guerrero, F. G. Aliev, R. Villar, J. Hauch, M. Fraune, G. Güntherodt, K. Rott, H. Brückl, and G. Reiss, *Appl. Phys. Lett.* **87**, 042501 (2005).

- <sup>5</sup>A. Gibson, R. Haydock, and J. P. LaFemina, *J. Vac. Sci. Technol. A* **10**, 2361 (1992).
- <sup>6</sup>A. Pojani, F. Finocci, J. Goniakowski, and C. Noguera, *Surf. Sci.* **387**, 354 (1997).
- <sup>7</sup>J. Goniakowski, C. Noguera, and L. Giordano, *Phys. Rev. Lett.* **93**, 215702 (2004).
- <sup>8</sup>J. Goniakowski, C. Noguera, and L. Giordano, *Phys. Rev. Lett.* **98**, 205701 (2007).
- <sup>9</sup>J. Goniakowski, L. Giordano, and C. Noguera, *Phys. Rev. B* **81**, 205404 (2010).
- <sup>10</sup>W. I. Park, D.-H. Kim, G.-C. Yi, and C. Kim, *Jpn. J. Appl. Phys.* **41**, 6919 (2002).
- <sup>11</sup>H. Kato, K. Miyamoto, M. Sano, and T. Yao, *Appl. Phys. Lett.* **84**, 4562 (2004).
- <sup>12</sup>R. Arita, Y. Tanida, S. Entani, M. Kiguchi, K. Saiki, and H. Aoki, *Phys. Rev. B* **69**, 235423 (2004).
- <sup>13</sup>Z. Vashaei, T. Minegishi, H. Suzuki, M. W. Cho, and T. Yao, *Phys. Status Solidi C* **3**, 1042 (2006).
- <sup>14</sup>M. Xue and Q. Guo, *J. Chem. Phys.* **127**, 054705 (2007).
- <sup>15</sup>T. Susaki, S. Kumada, T. Katase, K. Matsuzaki, M. Miyakawa, and H. Hosono, *Appl. Phys. Express* **2**, 091403 (2009).
- <sup>16</sup>H. T. Yuan, Y. Z. Liu, Z. Q. Zeng, Z. X. Mei, Y. Guo P. Zhang, X. L. Du, J. F. Jia, Z. Zhang, and Q. K. Xue, *J. Cryst. Growth* **311**, 425 (2009).
- <sup>17</sup>K. Matsuzaki, H. Hosono, and T. Susaki, *Phys. Rev. B* **82**, 033408 (2010).
- <sup>18</sup>S. Benedetti, N. Nilius, P. Torelli, G. Renaud, H.-J. Freund, and S. Valeri, *J. Phys. Chem. C* **115**, 23043 (2011).
- <sup>19</sup>V. K. Lazarov, Z. Cai, K. Yoshida, K. H. Zhang, M. Weinert, K. S. Ziemer, and P. J. Hasnip, *Phys. Rev. Lett.* **107**, 056101 (2011).
- <sup>20</sup>P. A. Stampe, M. Bullock, W. P. tucker, and R. J. Kennedy, *J. Phys. D: Appl. Phys.* **32**, 1778 (1999).
- <sup>21</sup>W. R. L. Lambrecht, S. Limpijumnong, and B. Segall, *MRS Internet J. Nitride Semicond. Res.* **4S1**, G6.8 (1999).
- <sup>22</sup>D. Wu, M. G. Lagally, and F. Liu, *Phys. Rev. Lett.* **107**, 236101 (2011).
- <sup>23</sup>C. Martínez-Boubeta, J. I. Beltrán, L. Balcells, Z. Konstantinović, S. Valencia, D. Schmitz, J. Arbiol, S. Estrade, J. Cornil, and B. Martínez, *Phys. Rev. B* **82**, 024405 (2010).
- <sup>24</sup>I. Slipukhina, Ph. Mavropoulos, S. Blügel, and M. Ležaić, *Phys. Rev. Lett.* **107**, 137203 (2011).
- <sup>25</sup>E. Kan, F. Wu, Y. Zhang, H. Xiang, R. Lu, C. Xiao, K. Deng, and H. Su, *Appl. Phys. Lett.* **100**, 072401 (2012).
- <sup>26</sup>Ll. Balcells, J. I. Beltrán, C. Martínez-Boubeta, Z. Konstantinović, J. Arbiol, and B. Martínez, *Appl. Phys. Lett.* **97**, 252503 (2010).
- <sup>27</sup>D. X. Liu, F. Iza, X. H. Wang, M. G. Kong, and M. Z. Rong, *Appl. Phys. Lett.* **98**, 221501 (2011).
- <sup>28</sup>K. Schwarz and P. Blaha, *Comput. Mater. Sci.* **28**, 539 (2003).
- <sup>29</sup>E. Sjöstedt, L. Nordström, and D. J. Singh, *Solid State Commun.* **114**, 15 (2000).
- <sup>30</sup>Z. Wu and R. E. Cohen, *Phys. Rev. B* **73**, 235116 (2006).
- <sup>31</sup>P. Haas, F. Tran, and P. Blaha, *Phys. Rev. B* **79**, 085104 (2009).
- <sup>32</sup>For a review on formation of heteroepitaxial domains, see M. Grundmann, *Phys. Status Solidi B* **248**, 805 (2011).
- <sup>33</sup>C. Martínez-Boubeta, A. Martínez, S. Hernández, P. Pellegrino, A. Antony, J. Bertomeu, Ll. Balcells, Z. Konstantinović, and B. Martínez, *Solid State Commun.* **151**, 751 (2011).
- <sup>34</sup>O. Jambois, P. Carreras, A. Antony, J. Bertomeu, and C. Martínez-Boubeta, *Solid State Commun.* **151**, 1856 (2011).
- <sup>35</sup>H. Sieber, D. Hesse, X. Pan, St. Senz, and J. Heydenreich, *Z. Anorg. Allg. Chem.* **622**, 1658 (1996).
- <sup>36</sup>K. Lehovec, *J. Chem. Phys.* **21**, 1123 (1953).
- <sup>37</sup>M. Backhaus-Ricoult, *Annu. Rev. Mater. Res.* **33**, 55 (2003).
- <sup>38</sup>K. Matsuzaki, H. Takagi, H. Hosono, and T. Susaki, *Phys. Rev. B* **84**, 235448 (2011).
- <sup>39</sup>S. Limpijumnong and W. R. L. Lambrecht, *Phys. Rev. B* **63**, 104103 (2001).
- <sup>40</sup>K. Nagashima, T. Yanagida, H. Tanaka, and T. Kawai, *J. Appl. Phys.* **101**, 026103 (2007).
- <sup>41</sup>V. Pardo and W. E. Pickett, *Phys. Rev. B* **81**, 035111 (2010).
- <sup>42</sup>M. Grünwald, E. Rabani, and C. Dellago, *Phys. Rev. Lett.* **96**, 255701 (2006).